

Cesium saturation spectroscopy revisited: How to reverse peaks and observe narrow resonances

O. Schmidt, K.-M. Knaak, R. Wynands, D. Meschede

Institut für Quantenoptik, Universität Hannover, Welfengarten 1, D-30167 Hannover, Germany
(Fax: +49-511/762-2211)

Received 5 March 1994/Accepted 9 May 1994

Abstract. The complex magnetic structure of the cesium atom is responsible for the interesting behaviour of its saturated absorption spectra, e.g., a two-fold sign reversal of a crossover resonance, under various polarization configurations with and without applied magnetic fields. We show that this morphology is a result of optical pumping processes including coherent population trapping which, under normal laboratory conditions, prevent the atoms from reaching an equilibrium situation. Our interpretation is useful for an intuitive and rapid understanding of this important tool in high-resolution spectroscopy.

PACS: 32.80.Bx, 42.65. Ft

The application of saturated absorption of a narrowband laser light source in alkali vapor gas cells is commonplace in many laboratories. This instrument is one of the simplest devices of high-resolution spectroscopy and routinely used as a frequency reference. In recent years cesium and rubidium vapors have become particularly important since narrowband laser diodes are now readily available for their D_2 -resonance wavelengths at 852 nm and 780 nm, respectively. They are widely applied to many mainstream lines of research in quantum optics such as magneto-optic trapping. While numerous reference spectra have been published, little attention has been given to the details of the spectrum. With an unrealistic two-level atom in mind naive estimates could, for instance, expect the ($F=4 \rightarrow F'=5$) transition to be most prominent because of statistical weights, contrary to observation.

The important role of optical pumping [1–3] in saturation spectroscopy has in fact been realized [4–7] more than a decade ago, and an in-depth theoretical analysis has been applied by Nakayama [8] to cesium and rubidium. In the meantime, coherence properties of diode lasers for several laboratory applications have tremendously improved [9, 10], and the resolution of saturated absorption spectroscopy went up accordingly.

In this communication we will collect and analyze in detail the morphology and intensities of the important cesium D_2 -saturation spectrum with emphasis on the delicate interaction of atomic magnetism, external magnetic fields, and light fields. For selected examples we will show that spectral properties of the nonlinear radiation interaction are well predicted by a simplified theory. It is our main intention to give simple physical interpretations for the observed spectra which are useful for an intuitive understanding of this common high-resolution laboratory device. Since cesium with its nuclear spin of $I=7/2$ is the most complex alkali atom, the results can be transferred to all alkali spectra.

1 Saturated absorption spectrometer

The experimental setup is the standard configuration for saturated absorption spectroscopy (Fig. 1). A semiconductor laser diode (STC LT50A-03U, 852 nm) is optically stabilized by feedback from a confocal Fabry-Perot resonator [9]. With a thick uncoated glass plate two weak beams of variable diameter are split off and sent through a cesium vapor cell onto a pair of photodiodes. An

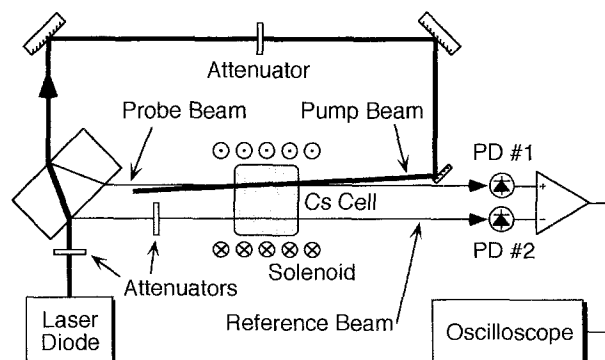


Fig. 1. Experimental setup for saturated absorption spectroscopy in magnetic fields (PD: photodiode)

optical attenuator in the reference beam is used to equalize the two intensities. The main part of the beam is sent through the cell from the other direction and carefully aligned so as to overlap the probe beam over its whole length inside the cell. Its power can be adjusted with another optical attenuator. The cell itself is cylindrical with a diameter of 25 mm, a length of 20 mm, and two windows perpendicular to the laser beams. The cell is at ambient temperature and is placed inside an arrangement of three mutually orthogonal induction coil pairs, so that stray magnetic flux densities can be compensated to within better than 10 mG over the entire volume of the cesium cell. An additional solenoid can produce longitudinal (i.e., parallel to the laser beams) magnetic flux densities of up to 20 G. An instrumentation amplifier is used to subtract the signal of photodiode #2 from that of photodiode #1. This output signal is then monitored on a storage oscilloscope.

Common laboratory jargon calls this arrangement a saturated-absorption spectroscopy setup [11]. The explanation usually given is that the strong pump beam saturates a transition and the weak probe beam probes

this change in atomic population. Since both beams are derived from the same laser and thus have the same frequency, the Doppler effect brings different velocity groups into resonance with each beam. Consequently, the probe beam sees the hole burnt into the population difference by the pump beam only for those atoms that fly perpendicularly to the laser beam (" $v=0$ "-resonance). All other velocity groups contribute a Doppler background which is electronically subtracted using the reference beam.

2 Zero-field results

The spectra of Fig. 2 were recorded under standard laboratory conditions with the important exception of a well-compensated stray magnetic field. In this figure and all other spectra a positive peak means enhanced transmission for the probe beam under the influence of the pump beam, and a negative peak means increased absorption. The positions of the nonlinear resonances are straightforwardly understood from a diagram of the re-

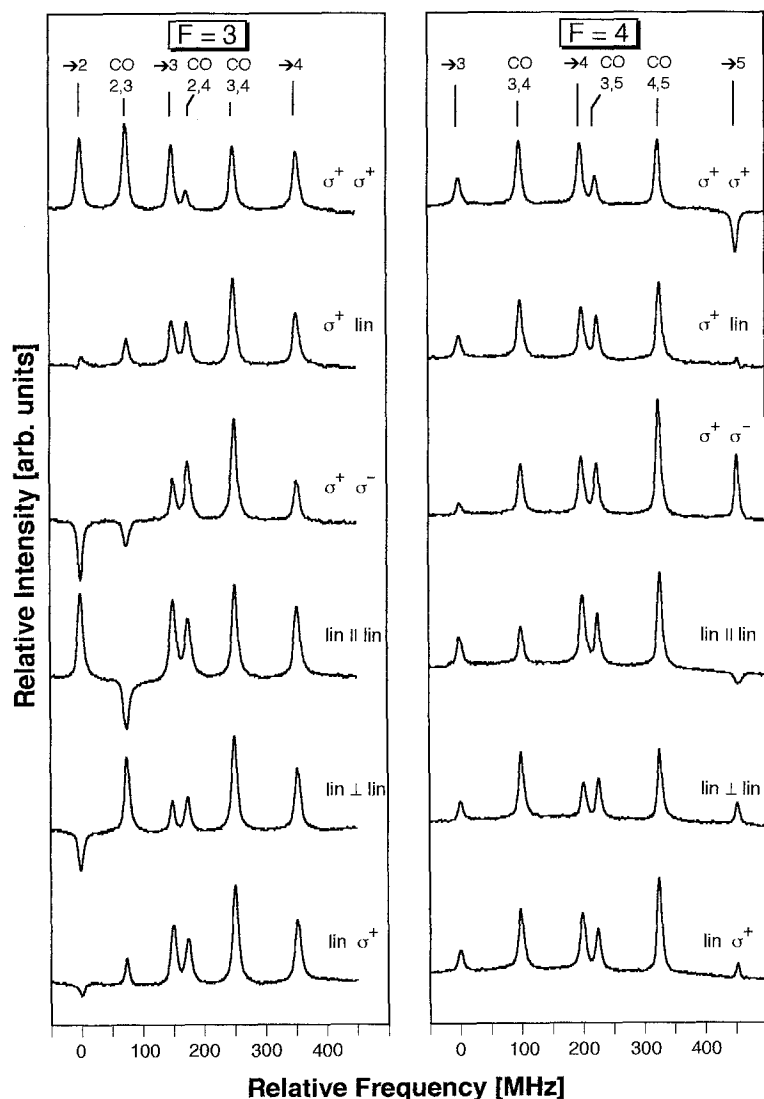


Fig. 2. Typical experimental saturated absorption spectra in zero magnetic field for various polarizations of pump and probe beams. All spectra are shown to the same scale and were taken with all parameters unchanged except for the laser polarizations. Next to each spectrum the polarization configuration is given. For example, " σ^+ lin" means σ^+ polarized pump and linearly polarized probe beam. On the left-hand side the spectra for transitions starting from the lower ($F=3$) level are shown, those from the ($F=4$) level can be seen on the right-hand side. All transitions are identified at the top of the diagram. " $\rightarrow 3$ " stands for the $v=0$ resonance to level ($F'=3$), " $\text{CO } 2, 3$ " for the crossover resonance between the $3 \rightarrow 2$ and the $3 \rightarrow 3$ transitions. Note that not only the intensities of the lines change but sometimes also their signs

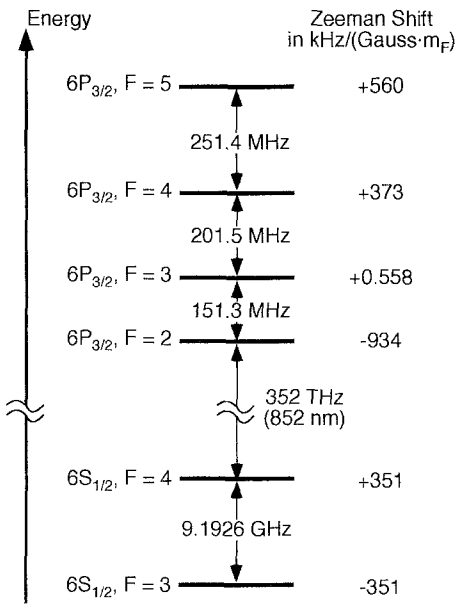


Fig. 3. Levels participating in the cesium D_2 -resonance, their frequency differences, and their Zeeman shifts

levant levels in cesium (Fig. 3). Three dipole-allowed transitions arise from the $v=0$ combined interaction of pump and probe beam. Three more peaks in Fig. 2 marked “CO” (CrossOver) are found exactly midway between two $v=0$ -resonances. In this case, for a certain velocity group, one of the transitions is Doppler-shifted into resonance with the pump beam and the other one into resonance with the probe beam, leading again to simultaneous interaction with both light fields. A second group with opposite velocity component along the probe beam contributes indistinguishably to this resonance with exchanged roles of pump and probe beam. Figure 2 clearly shows that the appearance of the Doppler free spectra can be strongly varied by controlling the polarizations of pump and probe beam [12]. This is most notable in a change of sign from *enhanced transmission* to *enhanced absorption* in certain transitions.

An important parameter in our experiments is the saturation intensity $I_{\text{sat}} = 2\pi\hbar c\Gamma/\lambda^3$ which is the laser intensity required to drive stimulated emission at the same rate as spontaneous emission. For the $(F=4, m_F = \pm 4 \rightarrow F=5, m_F = \pm 5)$ transition this occurs at

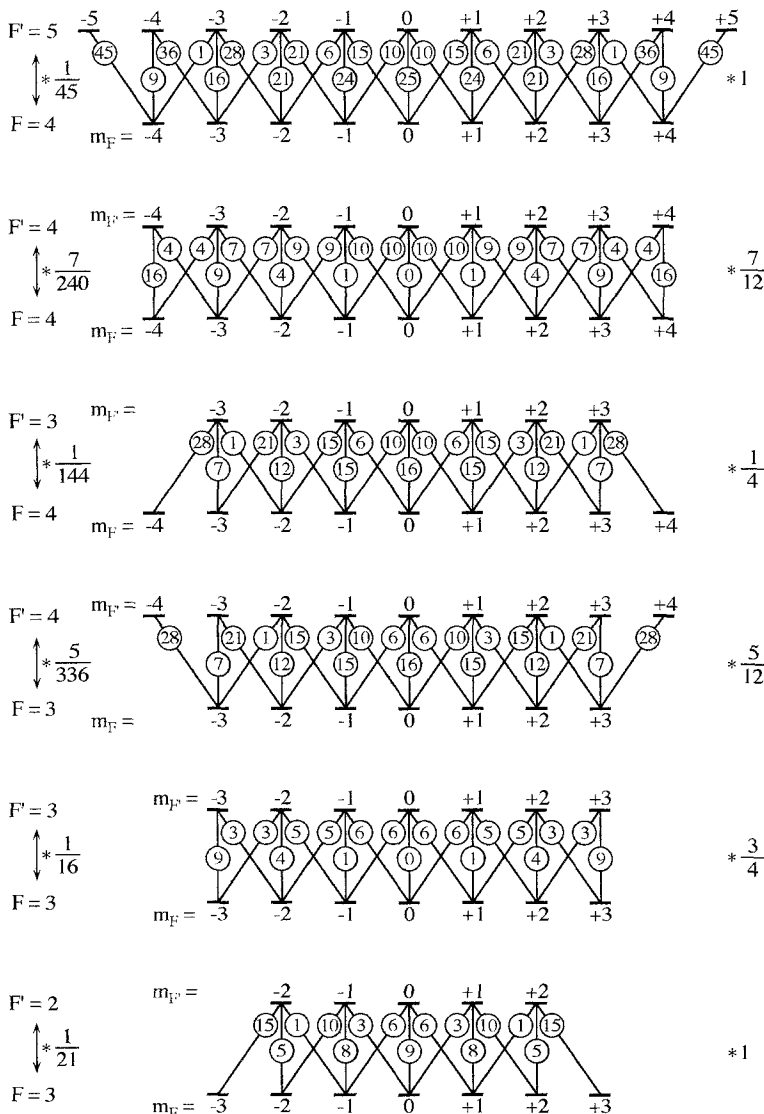


Fig. 4. Normalized transition probabilities between all magnetic sublevels in the cesium D_2 -resonance line. The factors on the right give the total statistical weight of the transition between levels F and F' . For example, the $(F'=5)$ level can only decay to the $(F=4)$ level, whereas the $(F'=4)$ level decays into $(F=3)$ with a total probability of $5/12$ and into $(F=4)$ with a total probability of $7/12$. The numbers printed in the small circles on each transition have to be multiplied by the factor on the left-hand side of the diagram. They give the branching ratios to individual magnetic sublevels within the $(F \rightarrow F')$ transition. For example, the $(F'=4, m_F=0)$ sublevel decays into $(F=4, m_F = \pm 1)$ with $10 \times 7/240$ probability each. Note that the normalization is done such that the total probabilities for the decay of any individual level are 1. For example, the $(F'=4, m_F=0)$ total decay rate is $(10+0+10) \times 7/240 + (6+16+6) \times 5/336 = 7/12 + 5/12 = 1$.

$I_0 = 1.1 \text{ mW/cm}^2$. In our experiments we have kept optical intensities below 0.1 mW/cm^2 , or $1/10$ of the saturated absorption intensity, I_0 . At an intensity of I_0 , however, only the $(F=4, m_F = \pm 4 \rightarrow F'=5, m_{F'} = \pm 5)$ transition is really saturated. For the weaker transitions saturation occurs for much higher intensities, for instance at $45I_0$ for the $(F=4, m_F = \pm 4 \rightarrow F'=5, m_{F'} = \pm 3)$ transition (Fig. 4). In a gas cell atom-light-interaction not only reduces level population differences, but it also causes a variation of the interaction strength due to optical pumping effecting rotation of atomic magnetic moments. Our interpretation will show that in typical laboratory systems the latter mechanism usually dominates most aspects of the observed nonlinear spectra. The term *velocity selective optical pumping* suggested by Pinard et al. [4] seems indeed more appropriate. For a detailed investigation we will separately discuss four subsets of the saturated absorption resonances to show qualitatively different mechanisms of optical pumping. (i) In closed systems formed by the $(F=4 \rightarrow F'=5)$ and $(F=3 \rightarrow F'=2)$ transitions Zeeman optical pumping causes orientation and alignment of the atoms. (ii) When transitions $(F=4 \rightarrow F'=3, 4)$ or $(F=3 \rightarrow F'=3, 4)$ are excited spontaneous decay to the other ground state hyperfine component is possible causing depopulation pumping. (iii) Crossover resonances are more complex, because they involve two excited levels of different F' so that at least one of them can spontaneously decay into both ground states. Depopulation as well as Zeeman optical pumping are observable. (iv) Saturated absorption spectra involving both hyperfine components of the ground state can be realized by the application of two lasers at different frequency, leading to repopulation pumping.

To be specific about geometry we will use the Π and Σ frames shown in Fig. 5. The Π frame has the z -quantization axis orthogonal to the light beams. It is most

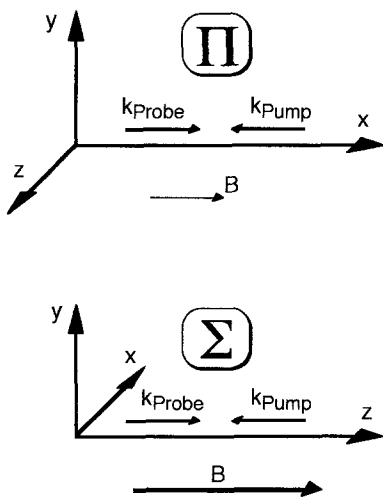


Fig. 5. Two coordinate systems used to explain the experimental spectra. The Σ system is most appropriate for the situation of relatively strong magnetic fields, whereas the Π system is very convenient for linear laser polarization in the low-field case

appropriate for discussing zero-field effects. In the Σ frame the z -axis is pointing along the propagation direction of the probe beam. This frame is more convenient when discussing magnetic-field influences introduced in the following chapter.

2.1 Resonances in closed systems: Zeeman pumping

The $(F=3 \rightarrow F'=2)$ transition corresponds to the low-frequency component in the traces on the left-hand side of Fig. 2. The influence of optical pumping is clearly visible in the difference between the $\sigma^+\sigma^+$ and the $\sigma^+\sigma^-$ configuration. The combined interaction $\sigma^+\sigma^+$ more efficiently populates the nonabsorbing $(m_{F=3} = +3)$ state than each of the individual beams and hence increases transmission. In the other case, however, σ^+ and σ^- counteract each other through the repopulation of absorbing Zeeman components, thereby increasing absorption. Similar arguments can be found for the qualitative aspects of the spectra involving linear polarizations. Hence, the intensity of the $(3 \rightarrow 2)$ resonance is dominantly a function of the number of atoms pumped into the nonabsorbing $m_F = 3$ component.

The closed transition $(F=4 \rightarrow F'=5)$ is certainly the most important subsystem of the cesium spectrum since it contains the two-level systems $(F=4, m_F = \pm 4 \rightarrow F'=5, m_{F'} = \pm 5)$. Optical pumping towards the $(F=4, m_F = 4)$ state increases the dipole coupling strength for σ^+ pump and σ^+ probe beam and is therefore responsible for the surprising increase of absorption. Conversely, a σ^- probe beam counteracts this pumping process, leading to a decrease of the effective dipole moment and hence an increase in transmission.

Note that in the series of spectra starting from $(F=4)$ the $(F=4 \rightarrow F'=5)$ transition is the only one to show a reversal of sign. The mere fact that we observe increased absorption on the $(F=4 \rightarrow F'=5)$ transition in the $\sigma^+\sigma^+$ configuration clearly indicates that this transition is not a pure two-level system under normal laboratory conditions. This is because usually the atoms do not spend enough time in the laser beam to reach an equilibrium situation with all atoms in the $(m_{F=4} = 4)$ component.

According to this interpretation the line strength has to depend both on pump beam intensity and also on interaction time since efficient optical pumping in a multilevel system requires many spontaneous emission cycles. The dependence on the rate of optical pumping is globally confirmed by the dependence of the resonance line shape and height on pump beam power. In Fig. 6 saturated absorption spectra of the $(F=4 \rightarrow F'=3, 4, 5)$ transition in $\sigma^+\sigma^+$ configuration are shown as a function of pump beam intensity. The $(4 \rightarrow 5)$ transition is especially interesting because it evolves from a shallow dip at low pump intensity to a narrow peak centered on a broad dip. With increasing intensity atoms are more frequently excited and hence more rapidly pumped to the extreme m_F -components, resulting in an enhanced absorption (Fig. 6; $r=0.27, r=1.3$). Since the power densities are now on the order of the saturation intensity we have to consider the effect of saturation in the recorded spectra.

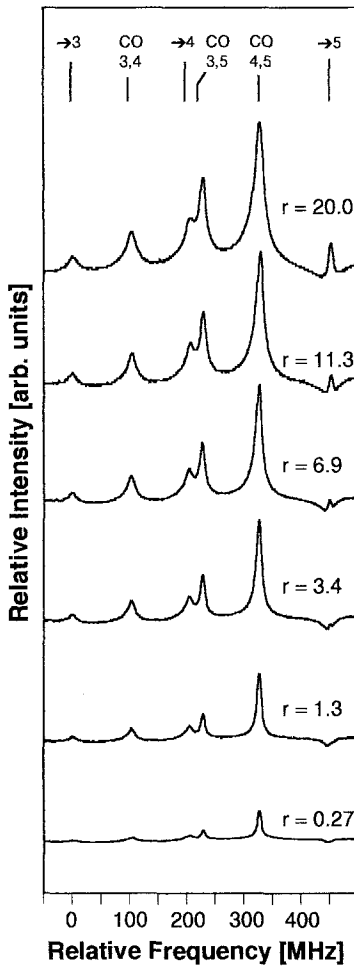


Fig. 6. Series of saturated absorption spectra starting from the ($F=4$) ground state taken with constant probe-beam intensity and successively weaker pump-beam intensity ($r = I_{\text{pump}}/I_{\text{probe}}$). The probe-beam intensity was of order I_0 . All spectra are to the same scale. The $F=4 \rightarrow F'=5$ transition shows a reversal of sign with decreasing pump intensity. The spectra of Figs. 2 and 10 were taken with $r=3$ and $I_{\text{probe}} = 0.4 \mu\text{W}/\text{mm}^2$

At even higher intensities the absorption coefficient decreases and results in a reversal of sign. Nonresonant laser light causes optical pumping as well but at a lower rate resulting in a situation completely analogous to the case of lower intensities with an increased absorption coefficient. Hence one observes enhanced absorption in the vicinity of this resonance line. The narrow saturation peak is not centered on the broad optical pumping dip. This shift is induced by light pressure, which becomes important for the ($F=4 \rightarrow F'=5$) closed system [13, 14].

We obtained similar results when we tested the dependence on interaction time by varying the diameter of the laser beams, which had been investigated before by Rinneberg et al. [6].

2.2 Hyperfine depopulation pumping

The excited states ($F'=3, 4$) are spontaneously coupled to both the ($F=3$) and the ($F=4$) hyperfine component

of the ground state, while coherent interaction takes place with only one of the ground state levels. Hence every excitation involves a large probability of order $1/2$ for decay to the other, effectively nonabsorbing hyperfine state. This variant of optical pumping is usually called hyperfine depopulation pumping, and it efficiently reduces absorption strength already after a few optical cycles. The nonlinear resonances corresponding to these transitions are therefore frequently more prominent than the resonances corresponding to closed systems with larger statistical weight.

2.3 Crossover resonances

In a crossover resonance one of the ($F'=3, 4$) levels, which can decay to the other ground state, is inevitably excited. This is one of the reasons why crossover resonances also have considerable line strengths. The participation of nonabsorbing levels such as the ($F=3, m_F = \pm 3$) states in the (2, 3) crossover transition is again the origin of drastic changes of the resonance line with polarization configuration of pump and probe beam.

2.4 Hyperfine repopulation pumping

In saturated absorption spectroscopy of the cesium D_2 -line no crossover resonances involving both hyperfine ground state levels coupled to a single excited level appear. This is because the level spacing between the ($F=3$) and the ($F=4$) ground state is 9.2 GHz while the Doppler width measures only 500 MHz. Hyperfine structure depopulation and repopulation pumping between the ground states can be observed, however, by using two different lasers [15, 16]. We changed our experimental setup by removing the pump beam mirrors and using a second semiconductor laser stabilized by optical feedback (Fig. 7). One of the lasers is tuned to a fixed frequency near the $^2S_{1/2}(F=4) \rightarrow ^2P_{3/2}$ Doppler-broadened transition frequency and acts as a pump beam. The second laser is scanned across the $^2S_{1/2}(F=3) \rightarrow ^2P_{3/2}$ resonance and its transmission is recorded using two photodiodes. As in the saturated absorption spectroscopy setup we amplify the difference of the photocurrents in order to obtain a Doppler-free signal with an offset due to the pump laser intensity. As before, a peak indicates

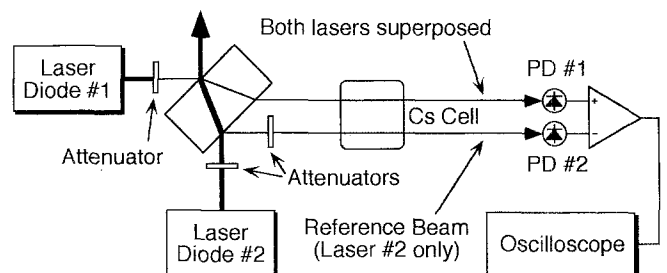


Fig. 7. Experimental setup for the observation of hyperfine repopulation pumping (PD: photodiode)

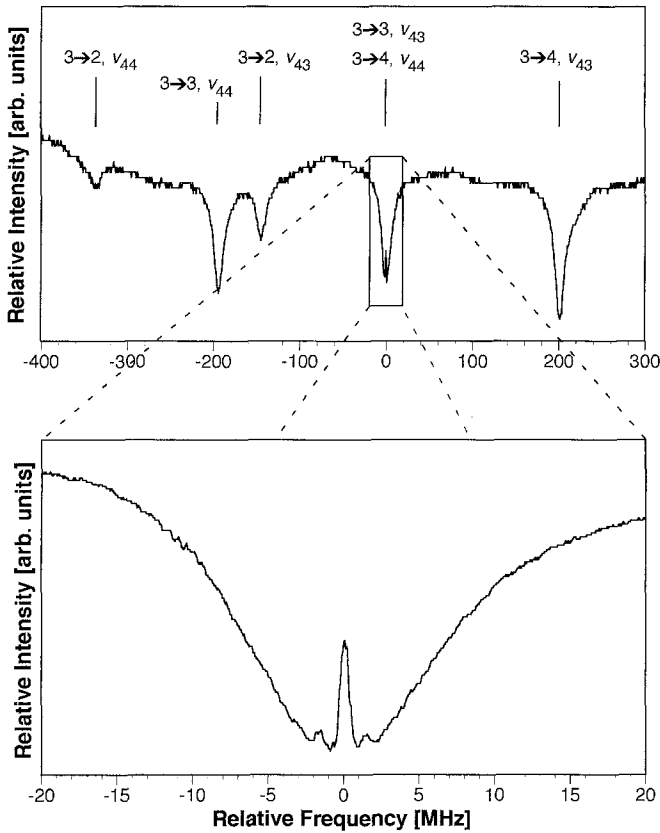


Fig. 8. Spectrum taken with the setup of Fig. 7. Laser #1 is tuned to the Doppler-broadened ($F=4 \rightarrow F'=3, 4, 5$) transition while laser #2 is scanned across the ($F=3 \rightarrow F'=2, 3, 4$) transition. The identification of the individual lines is explained in the text. The common $(3, 3)v_{43}$ and $(3, 4)v_{44}$ resonance is shown with better resolution in the lower part of the figure. The small bumps next to the narrow resonance peak are due to an intentional modulation of the laser current at a frequency of 1.5 MHz; they are used as frequency markers

enhanced transmission for the probe beam under the influence of the pump beam. Figure 8 shows a typical spectrum recorded with equal intensities and linear polarizations for pump and probe beam. Five resonances corresponding to enhanced absorption can be resolved. They are caused by a repopulation of the lower hyperfine level which is coupled to the probe laser field. Resonant excitation by the pump field at frequency $\omega_p = c|\mathbf{k}_p|$ followed by spontaneous emission to the lower hyperfine ground state is only possible in the ($F=4 \rightarrow F'=3, 4$) systems. The pump laser increases the population for two different velocity groups in this level:

$$\begin{aligned} v_{43} &= (\omega_p - \omega_{43})/k_p, \\ v_{44} &= (\omega_p - \omega_{44})/k_p. \end{aligned} \quad (1)$$

According to Fig. 9 two sets of three Doppler-free resonances each are expected. For the $(3, 4)v_{44}$ line pump and probe beam are coupled to the same excited level. Therefore, their difference frequency must be equal to the ($F=3 \rightarrow F=4$) 9.2 GHz hyperfine transition frequency of the cesium atom. The same argument holds for the $(3, 3)v_{43}$ line, so these two lines are degenerate.

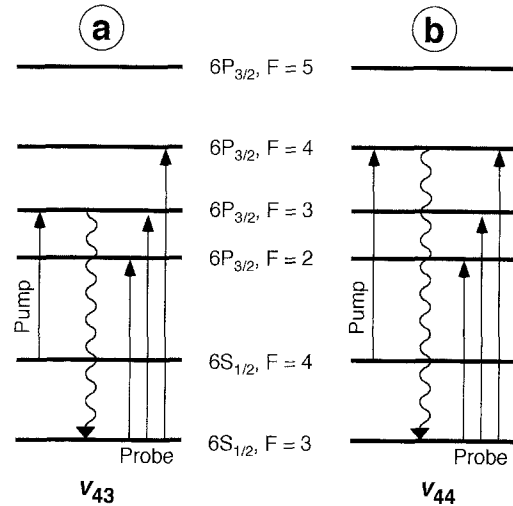


Fig. 9. Transitions involved in the generation of hyperfine repopulation pumping resonances. Explanation in text

This common resonance is the only one with coherent coupling between all participating levels. It shows a very narrow Raman-resonance line which will be explained in more detail in the last section.

3 Experimental and theoretical results in weak fields

3.1 Evolution of saturated absorption spectra in weak magnetic fields

In Fig. 10 we show the evolution of the saturated absorption spectrum of the ($F=3 \rightarrow F'=2, 3, 4$) transition for linear and parallel polarizations of pump and probe beam in a magnetic field parallel to the laser propagation. Two regimes of magnetic field influence are clearly distinguishable. Spectra on the left-hand-side of Fig. 10 show significant changes in the intensities of the various spectral components at magnetic flux density levels below 1 G, where Zeeman shifts remain much below the natural linewidth of 6 MHz. The right-hand side shows the regime from 1 G to 20 G where individual Zeeman components become more and more resolved. An unusually narrow dip which reverses the sign again is observed evolving from the zero-field (2, 3) crossover resonance. The ($F=3 \rightarrow F'=2, 3$) crossover resonance is composed of many possible combinations of transitions between magnetic sublevels, each one with a different Zeeman shift. The shift between neighboring transitions is 116 kHz/G. Therefore at 10 G this magnetic shift is still below the natural linewidth. Hence a magnetic multilevel system is coupled to the radiation field and optical pumping remains important.

The ($F=3 \rightarrow F'=4$) transition clearly exemplifies the other case, where the Zeeman shift between neighboring transitions is 725 kHz/G and hence the radiation field couples to nearly independent two-level systems.

We might mention here that the spectra obtained with an average uncompensated laboratory setup are similar in appearance to the 120 mG or 1 G traces of Fig. 10.

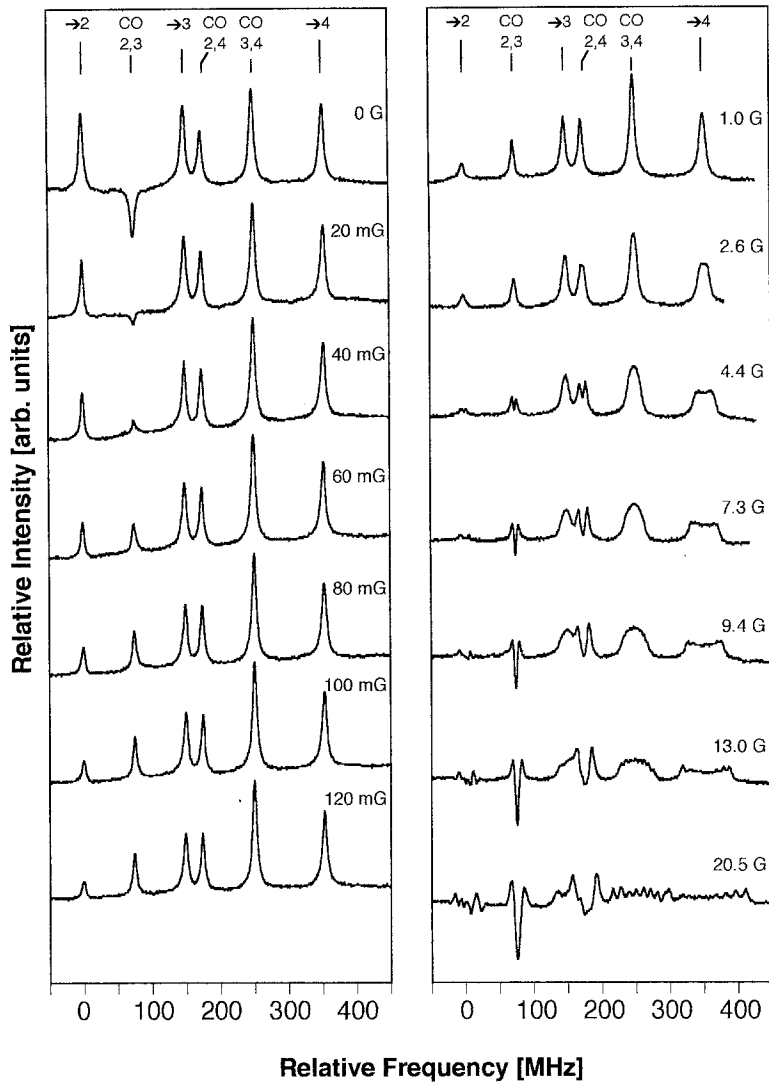


Fig. 10. Saturated absorption spectra of the transitions starting from ($F=3$) for the lin || lin configuration in successively stronger magnetic flux densities ($I_{\text{pump}} = 1.1 \mu\text{W}/\text{mm}^2$, $I_{\text{probe}} = 0.4 \mu\text{W}/\text{mm}^2$). Above a few G the Zeeman splitting starts to become resolved. Note the twofold peak reversal of the ($F=3 \rightarrow 2, 3$) crossover resonance

Let us discuss the influence of magnetic fields on the (2, 3) crossover resonance beginning with the II frame of Fig. 5. For $B=0$ the linearly polarized probe beam driving the ($3 \rightarrow 2$) transition accumulates atoms in the outermost ($m_F = \pm 3$) sublevels where they can no longer absorb light from the probe beam. These atoms are transferred back to an absorbing m_F level by the pump beam in resonance with the ($3 \rightarrow 3$) transition. This leads to enhanced absorption of the probe beam. For the other velocity group that contributes to the crossover resonance, i.e., atoms with opposite longitudinal velocity component, the pump beam is in resonance with the ($3 \rightarrow 2$) transition and optically pumps the atoms towards the ($m_F = \pm 3$) states. Since the ($F=3 \rightarrow F'=3$), $\Delta m=0$ transition is strongest for these states (Fig. 4), probe absorption is enhanced as well.

When a small magnetic field is applied along the propagation direction magnetic moments precess around the x -axis. This precession leads to a population redistribution among the m_F sublevels and therefore to enhanced transmission, since according to Fig. 4 lower $|m_F|$ levels have lower $\Delta m=0$ transition probabilities. This interpretation is valid as long as Zeeman shifts are small

compared to the resonance linewidth and hence differences in excitation strength are negligible for different m_F levels [6]. Stronger fields require a more general treatment which will be discussed in the following sections.

3.2 Rate-equation approximation

Because of their conspicuous behaviour we have selected the ($F=3 \rightarrow F'=2$) closed system and the ($F=3 \rightarrow F'=2, 3$) crossover resonance excited through linearly and parallel polarized pump and probe laser light for a demonstration of theoretical investigations. In order to calculate the nonlinear absorption spectrum we have to take the difference between the absorption coefficient α of the probe beam under the influence of the pump beam and the reference beam:

$$\alpha_{\text{nl}} = \alpha(\text{Probe + Pump}) - \alpha(\text{Reference}). \quad (2)$$

The absorption can be obtained from the density matrix ρ_{ij} by evaluating the expectation value of the the dipole operator

$$\alpha \propto \text{Re} \langle \hat{\mathbf{D}} \rangle = \text{Re} [\text{tr}(\hat{\mathbf{D}}\rho)]. \quad (3)$$

Here \hat{e} is the polarization direction and \mathbf{D} the atomic dipole operator. The density matrix itself is the solution of the equation of motion

$$i\hbar \frac{d\rho}{dt} = [H, \rho] + R,$$

$$H = H_a + V + H_{Zee}, \quad (4)$$

where R contains appropriate relaxation rates arising from, e.g., spontaneous emission. The total Hamiltonian H is a sum of the atomic Hamiltonian H_a and the coupling V with the light beam. The coupling with an external magnetic dipole field is taken into account by a linear weak field $H_{Zee} = g_F m_F \mu_B B$ operator. The calculation is carried out entirely in the Σ frame of Fig. 5. In this coordinate system the Zeeman Hamiltonian is diagonal while the light field introduces Zeeman coherences through optical pumping. Consequently, we have to calculate the full ground and excited state density matrices $\rho_{gg'}$ and $\rho_{ee'}$. For laser light polarized along the x -axis (Fig. 5)

$$\mathbf{E}(t) = E \hat{e}_x \text{Re}(e^{-i\omega t}) \quad (5)$$

the dipole operator in rotating wave approximation is

$$V = \frac{1}{2} (-E \hat{e}_x \mathbf{D}_{eg} e^{-i\omega t} - E^* \hat{e}_x \mathbf{D}_{ge} e^{i\omega t}). \quad (6)$$

\mathbf{D}_{eg} is defined by $\mathbf{D}_{eg} = |e\rangle \langle e| \mathbf{D} |g\rangle \langle g|$, where \mathbf{D} is the atomic dipole operator. In the rotating reference frame one obtains:

$$\begin{aligned} \dot{\rho}_{ee'} &= -i\Delta_{ee'} \rho_{ee'} - \gamma_r \rho_{ee'} - \Gamma \rho_{ee'} \\ &+ \frac{i}{\hbar} \sum_{g=e-1}^{e+1} (E \hat{e}_x \mathbf{D}_{eg} \tilde{\rho}_{ge'} - E^* \hat{e}_x \tilde{\rho}_{eg} \mathbf{D}_{ge'}), \\ \dot{\rho}_{gg'} &= -i\Delta_{gg'} \rho_{gg'} - \gamma_r \left(\rho_{gg'} - \frac{\delta_{gg'}}{2F+1} \right) + \sum_{ee'} \Gamma_{ee' gg'} \rho_{ee'} \\ &+ \frac{i}{\hbar} \sum_{e=g-1}^{g+1} (E^* \hat{e}_x \mathbf{D}_{ge} \tilde{\rho}_{e'g} - E \hat{e}_x \tilde{\rho}_{ge} \mathbf{D}_{e'g}), \\ \dot{\tilde{\rho}}_{eg} &= -i(\Delta_{eg} - \Delta_{\text{opt}}) \tilde{\rho}_{eg} - \gamma_r \tilde{\rho}_{eg} - \frac{1}{2} \Gamma \tilde{\rho}_{eg} \\ &+ \frac{i}{\hbar} \sum_{g'=e-1}^{e+1} E \hat{e}_x \mathbf{D}_{eg'} \rho_{g'e} \\ &- \frac{i}{\hbar} \sum_{e'=g-1}^{g+1} E^* \hat{e}_x \rho_{ee'} \mathbf{D}_{e'g}. \quad (7) \end{aligned}$$

Magnetic quantum numbers are e, e' for the excited state F' and g, g' for the ground state F . The difference of the Zeeman shifts of levels $|\alpha\rangle$ and $|\beta\rangle$ is called $\Delta_{\alpha\beta}$, while $\Delta_{\text{opt}} = \omega_L - \omega_{eg}$ is the detuning from exact resonance of the laser frequency ω_L in zero magnetic field. Γ is the

spontaneous decay rate and $\Gamma_{ee' gg'}$ is the spontaneous emission operator [3].

In a dilute vapor at some 10^{-5} mbar we can neglect collisional contributions and hence the relaxation of excited states ($\rho_{ee'}$) and optical coherences (ρ_{eg}) is dominated by spontaneous emission. Relaxation of ground state Zeeman coherences mainly results from atoms leaving the light field, while for atoms entering the beam in thermal equilibrium only ground state populations (ρ_{gg})_{th} = $1/(2F+1)$ are different from zero. We account for transit time effects through the introduction of a friction coefficient γ_r in (7). This results in a Lorentzian lineshape instead of an exponential variation with detuning [17]. This is of no concern, however, since our spectra are always limited by our laser linewidth of order 100 kHz. The transit-time broadening of order 10 kHz is calculated from $\Delta\omega_{\text{tot}}^{\text{HWHM}} = \gamma_r = \sqrt{2 \ln 2} \langle v \rangle_{\text{th}} / 2 \pi w$ where $\langle v \rangle_{\text{th}} = \sqrt{2 kT/m}$ is the average thermal velocity and w the (1/e)-width of a Gaussian laser beam. For cesium atoms at $T=300$ K one calculates $\gamma_r = 30 \times 10^3 \text{s}^{-1} / (w/\text{mm})$. Furthermore, we have replaced the Gaussian beam profile by a top-hat distribution of constant intensity I and diameter w . We also neglect the variation of beam intensities along the propagation axis, although we measured a total absorption of 50%.

Since we are only interested in a narrow spectral range in the vicinity of the nonlinear resonance we can also neglect coherent coupling of neighboring levels which are always more than 100 MHz away.

It is the main purpose of a conventional saturated absorption spectrometer to provide reference frequencies through narrow Doppler-free resonances. In order to avoid power broadening both pump and probe beam have to be restricted to low intensities, i.e. $I/I_0 \cong |E \cdot \mathbf{D}_{eg} / \hbar \Gamma|^2 \ll 1$. In this case the optical coherences adiabatically (i.e., $\dot{\tilde{\rho}}_{eg} \cong 0$) follow the evolution of the excited and ground state density matrices $\rho_{ee'}$ and $\rho_{gg'}$ which replaces the population difference in a two-level system.

In order to calculate a line profile we do not vary atomic velocities, but keep them fixed at their respective resonant values of $v_z=0$ for ($v=0$) resonances and of $v_{33} = \Delta\omega/2k$ and $v_{32} = -\Delta\omega/2k$ for the (2, 3)-crossover resonance, where $\Delta\omega$ is the spacing between the two participating upper levels. The variation of the laser frequency can be treated by detuning pump- and probe-beam frequencies from the crossover resonance frequency in the atomic rest frame. The influence of both pump and probe field can be treated in separate rotating wave frames, since we neglect coherent two-photon processes. A system of two sets of equations of motion according to (7) has to be solved, where the two sets are coupled through the density matrix elements. After a tedious but straightforward calculation a set of rate equations for the ground and excited state density matrices is obtained. A closely related method was used by Rinneberg et al. [6]. We numerically evaluated the resulting set of rate equations with a Runge-Kutta algorithm. Typical calculation times using a conventional personal computer are of order one hour for a line profile calculation with a grid of 50 frequency points.

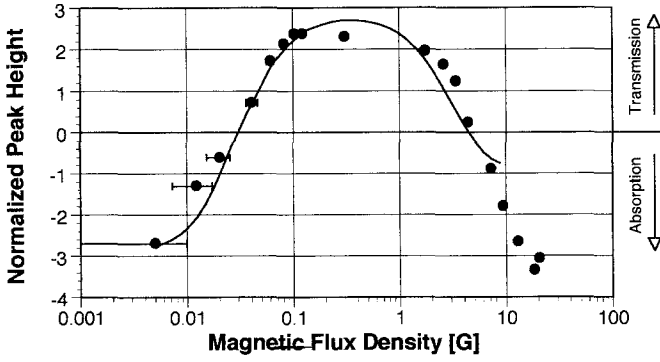


Fig. 11. Comparison of calculated (solid line) and measured height (dots) of the ($F=3 \rightarrow F'=2, 3$) crossover resonance peak for various magnetic flux densities. The error bars reflect the uncertainty in the measurement of the experimental flux density. Above 10 G, our approximation breaks down, as explained in text

3.3 Calculation of the resonant absorption coefficient

The results of the numerical calculation of the (2, 3) crossover resonance for various magnetic fields are shown in Fig. 11. The laser frequency is chosen to be exactly on resonance as described above and the peak height is scaled such that experiment and calculation coincide at zero field. For the calculation we used the measured ratio of pump and probe beam intensities incident onto the vapor cell. The absolute value, however, had to be reduced by 50% in order to obtain the best agreement between experiment and calculation. This is not surprising in view of the severe approximations we made for the beam profile. The calculations show a good agreement with our experimental results over a range of magnetic flux densities from zero field up to 7 G (Fig. 11). For higher magnetic flux densities the Zeeman splitting of the participating transitions becomes larger than the linewidth and our approximation of considering only one velocity group no longer holds since crossover resonances between the splitted transitions have to be taken into account.

3.4 The role of coherent population trapping in saturated absorption spectroscopy

The interpretation of the resonances in the Π frame is valid as long as the Zeeman shifts are small compared to the linewidth. In order to understand the behaviour in higher magnetic fields one usually chooses the Σ system, where the magnetic sublevels are eigenstates for the atomic energy in a magnetic field. A linear polarization along the Σ system's x -axis has to be described as a coherent superposition of σ^+ and σ^- polarized light.

Let us begin with a reinterpretation of the ($3 \rightarrow 2$) transition. As explicated for the Π system, optical pumping into the nonabsorbing magnetic sublevels ($m_F = \pm 3$) plays a dominant role. With a suitable transformation the "dark" states $|DS_1\rangle_{\Pi} = |m_F = 3\rangle$ and $|DS_2\rangle_{\Pi} = |m_F = -3\rangle$ in the Π system can be written as

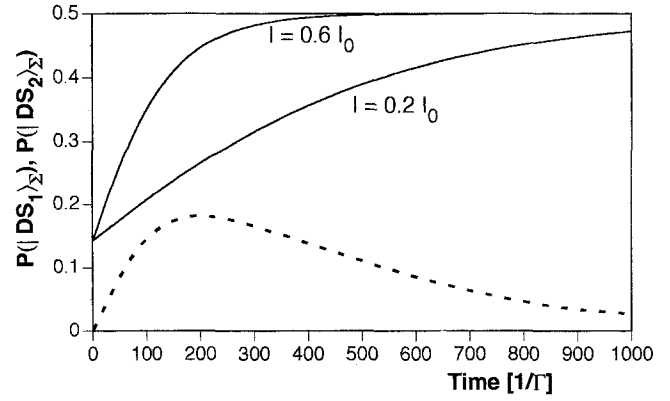


Fig. 12. Time evolution of the occupation probability of both dark states for the ($3 \rightarrow 2$) transition in the Σ system, calculated for two different laser intensities. The dashed line shows the difference of the two solid lines. Discussion in text

$$|DS_1\rangle_{\Sigma} = \frac{\sqrt{2}}{8} (|3\rangle + \sqrt{15}|1\rangle + \sqrt{15}|-1\rangle + |-3\rangle),$$

$$|DS_2\rangle_{\Sigma} = -\frac{\sqrt{2}}{8} (\sqrt{6}|2\rangle + \sqrt{20}|0\rangle + \sqrt{6}|-2\rangle) \quad (8)$$

in the Σ frame. $|DS_1\rangle_{\Sigma}$ and $|DS_2\rangle_{\Sigma}$ are nonabsorbing states for light polarized parallel to the Σ system's x -axis.

For laser light in resonance with the ($3 \rightarrow 2$) transition the absorption vanishes for infinite interaction time. Therefore, the nonlinear absorption coefficient for the ($F=3 \rightarrow F'=2$) transition vanishes, too. Figure 12 shows the numerically calculated probability of the dark states' population $P(|DS_1\rangle_{\Sigma})$ and $P(|DS_2\rangle_{\Sigma})$ for two different intensities as a function of time. (In (7) we have set $\gamma_r = 0$ for this evaluation.) The population approaches a maximum value of $1/2$ for each state. The rate of optical pumping into the dark states depends on the light intensity, of course. The dashed curve in Fig. 12 shows the difference of the dark state populations in a strong and a weak light beam as a function of interaction time. This is, in fact, our experimental situation where the reference beam is the weaker beam and the combination of pump and probe beam is the stronger one. When we take the difference of the photocurrents of PD #2 and PD #1 (Fig. 1) we see the nonlinear absorption signal. Its height is related to the value of the dashed curve for a time corresponding to the mean interaction time of an atom with one of the beams. This means that for finite interaction times there is absorption although there is none for $t \rightarrow \infty$. The observation of absorption on the ($F=3 \rightarrow F'=2, 3$) resonance clearly shows that the atoms do not reach the equilibrium situation in the typical experimental geometry.

Optical pumping into dark states is the well-known effect of coherent population trapping [18, 19, 20] in a three-level A system, where two levels $|g\rangle$ and $|g'\rangle$ are coupled to an excited level $|e\rangle$ by two laser fields close to resonance. Population trapping occurs if the laser frequencies fulfill a Raman condition $\omega_1 - \omega_2 = \Delta$, where Δ is the level spacing between $|g\rangle$ and $|g'\rangle$.

In our case the laser fields are the σ^+ and σ^- components of the linear-polarized light, which have the same frequency ω_L and a nearly perfect phase coherence. The width of the coherent population trapping resonance in frequency space is determined by the time-of-flight broadening in our gas cell ($\Delta\omega^{\text{HWHM}}/2\pi = 10$ kHz for a $w = 3$ mm beam). Of course, in our experimental setup it is not possible to detune the frequency of the σ^- component independently of the σ^+ frequency, but a small magnetic field along the quantization axis introduces a Zeeman shift which leads to an equivalent situation. For the $(3 \rightarrow 2)$ transition an efficient pumping process exists in zero magnetic field due to population trapping as described above. Hence, the line strength of the resonance is comparable to resonances where hyperfine pumping processes occur, e.g., $(3, 4)$ crossover, $(3 \rightarrow 3)$, $(3 \rightarrow 4)$. It can be seen that in small magnetic fields (30 mG) with a level shift on the order of the time-of-flight broadening of the coherent population trapping resonance the signal strength decreases rapidly for the $(3 \rightarrow 2)$ resonance line. With increasing magnetic flux densities the effect of coherent population trapping vanishes and resonance lines with hyperfine pumping show much more contrast.

To understand the behavior of the $(3, 2)$ crossover resonance one has to realize that for the $(3 \rightarrow 3)$ transition the states $|DS_1\rangle_{\mathcal{E}}$ and $|DS_2\rangle_{\mathcal{E}}$ are not “dark” but show

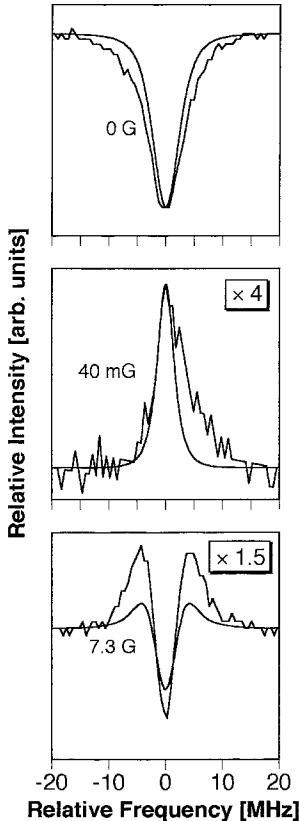


Fig. 13. Comparison of calculated (smooth curves) and experimental line shapes for the $(F=3 \rightarrow F'=2, 3)$ crossover resonance in magnetic flux densities of 0 G, 40 mG, and 7.3 G. The lower two figures were scaled by a factor of 4 and 1.5, respectively

a very strong absorption, which can be easily seen in the Π frame, where the $(m_F = \pm 3)$ levels show the strongest $\Delta m = 0$ transition probabilities.

3.5 Calculation of line profiles

In order to understand the line profiles we calculated the crossover absorption as a function of laser frequency for three magnetic flux densities (Fig. 13): in zero magnetic field (top) and near the zero point of the peak intensity in small fields (center) and in higher magnetic fields (bottom). The calculated profiles are plotted together with the corresponding measured profiles. It can be seen that the qualitative modifications over a large range of magnetic flux densities are correctly predicted.

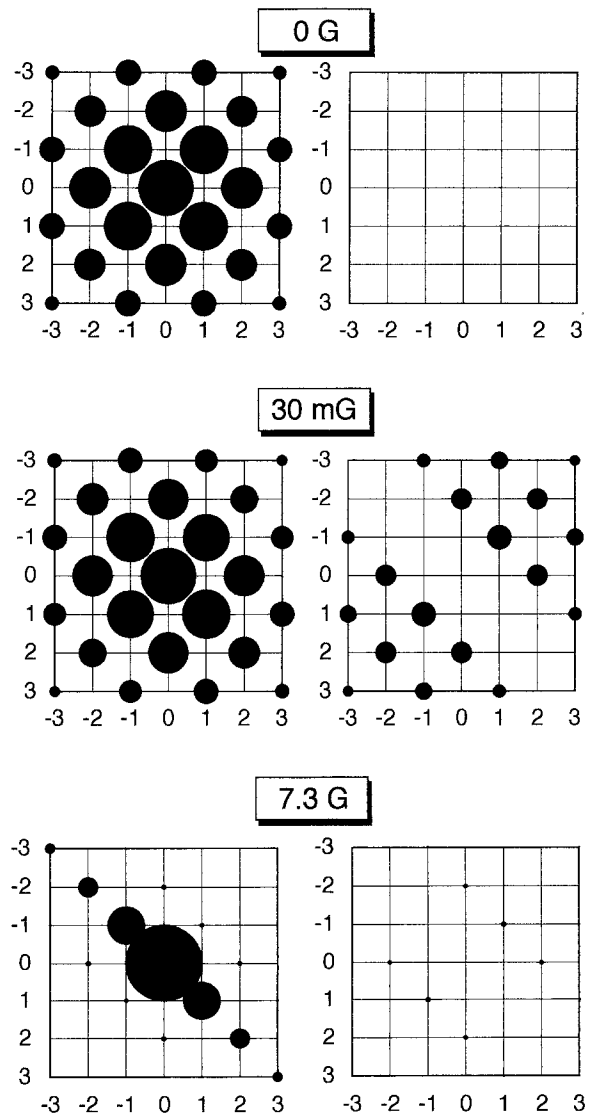


Fig. 14. Calculated density matrices of the $(F=3)$ ground state for various magnetic flux densities and $t \rightarrow \infty$. The area of each circle is proportional to the absolute value of the corresponding density matrix element connecting two of the magnetic sublevels. The matrices on the left show the real parts, those on the right the imaginary parts

We can interpret the interesting line shape at 7.3 G with the help of the ground state density matrix. Figure 14 shows results of the calculation for $t \rightarrow \infty$ for an atom entering a light field resonant with the $(3 \rightarrow 2)$ transition. In the zero field case the trapping states $|DS_1\rangle_Z$ and $|DS_2\rangle_Z$ are populated with a probability of 1/2 each. No imaginary parts of the coherences occur which shows that the dark states are eigenstates of the system. With a low flux density (30 mG) the coherences are no longer real and the resulting states cease to be eigenstates of the system. Figure 14 also shows the density matrix for a magnetic flux density of 7.3 G. It can be seen that we have an almost complete collapse of coherences. In this regime the coherence between the σ^- and σ^+ component of the linear polarized light is irrelevant. This is because with a Zeeman level shift comparable to the linewidth linearly polarized light will no longer excite coherences between ground state Zeeman sublevels. For a laser frequency equal to the zero field $(3 \rightarrow 2)$ transition frequency there is optical pumping to the inner sublevels where we have the strongest absorption for σ^+ and σ^- polarized light ($\Delta m = \pm 1$) to the $(F=3)$ excited state (Fig. 4). We have tested this interpretation by rotating the polarization direction of the pump beam continuously from the $\text{lin} \parallel \text{lin}$ to the $\text{lin} \perp \text{lin}$ configuration and did not see any change in the line shape or peak intensity, contrary to the zero field situation (Fig. 2).

4 Population trapping in ground-state hyperfine pumping

In ground state hyperfine pumping with the experimental setup of Fig. 7 a narrow dip appears in the line center of the degenerate $(3, 3)_{v43}$ and $(3, 4)_{v44}$ resonance [15, 16]. It is shown with better resolution in the bottom part of the figure. This narrow resonance corresponds to the coherent population trapping of the atomic population. Atoms are optically pumped into a coherent superposition of both ground states. This coherent superposition remains nonabsorbing for the applied radiation fields if the difference of the laser frequencies $\omega_{12} = \omega_1 - \omega_2$ is exactly equal to the level spacing of the two participating ground state levels. Since spontaneous decay and collisional relaxation are negligible compared to the time-of-flight broadening the width of the coherent population trapping resonance is determined by $\Delta\omega_{\text{tot}}/2\pi \cong 50$ kHz for our experimental setup. This is the minimum observable linewidth without fluctuations of the laser's difference frequency and power broadening. For copropagating laser beams the Doppler shift $\Delta_D\omega_{12} = (k_1 - k_2)v_z$ for an atom with axial velocity v_z is negligible anyway. Hence, population trapping occurs for all velocity groups v_z simultaneously. The contrast of the resonance is almost 50% while the linewidth of 700 kHz is determined by power broadening. With decreasing light intensities the linewidth and the contrast decrease. The influence of laser polarization, applied magnetic fields, and the laser intensity has been investigated in detail by Akulshin et al. [15] in a similar experiment with rubidium vapor.

Finally we want to focus on the question why we cannot see coherent population trapping resonances in the saturated absorption spectroscopy setup of Fig. 1. For example, with a σ^+ probe beam and a σ^- pump beam at the $(F=3 \rightarrow F'=2)$ transition frequency, which corresponds to the coherent population trapping configuration, no such resonances can be resolved (Fig. 2). Since the ground-state relaxation due to collisions or radiative decay can be neglected the width of the population trapping resonance in this case is again determined by time-of-flight broadening. This width (of order 10 kHz) is small compared to the linewidth of the transition frequency (of order 10 MHz). Since the laser beams are counterpropagating the Doppler effect prohibits population trapping except for a small range of velocities. In comparison with the Bennet hole of conventional saturated absorption spectroscopy the population trapping contribution to the spectrum is only of order 10 kHz/10 MHz = 1/1000. Population trapping occurs if the difference of the laser frequencies lies within the width of the coherent population trapping resonance, while the absolute laser frequencies determine the efficiency to populate the resonance. Since the efficiency is almost a Lorentzian distribution with a width given by the optical decay rate coherent population trapping changes the shape and the height of the Doppler-free resonance by 1/1000, which we cannot resolve experimentally. We should note, however, that the effect can be used as an efficient sub-Doppler cooling mechanism, the "velocity selective coherent population trapping" [21].

Acknowledgements. The authors wish to thank the Deutsche Forschungsgemeinschaft and the Graduiertenkolleg "Photonen, atomare Teilchen und deren Wechselwirkungen" for financial support.

References

1. W. Happer: Rev. Mod. Phys. **44**, 169 (1972)
2. W. Happer, W.A. van Wijngaarden: Hyperfine Interactions **38**, 435 (1987)
3. C. Cohen-Tannoudji: *Frontiers in Laser Spectroscopy*, ed. by R. Balian, S. Haroche, S. Liberman, Vol. 1 (North-Holland, Amsterdam 1977) p. 3
4. M. Pinard, C.G. Arimoff, F. Laloë: Phys. Rev. A **19**, 2366 (1979)
5. M.S. Feld, M.M. Burns, T.U. Kühl, P.G. Pappas, D.E. Murnick: Opt. Lett. **5**, 79 (1980)
6. H. Rinneberg, T. Huhle, E. Matthias, A. Timmermann: Z. Phys. A **295**, 17 (1980)
7. M.D. Levenson, S.S. Kano: *Introduction to Nonlinear Laser Spectroscopy*, 2nd edn. (Academic, London 1988)
8. S. Nakayama: Jpn. J. Appl. Phys. **24**, 1 (1985) and references therein
9. B. Dahmani, L. Hollberg, R. Drullinger: Opt. Lett. **12**, 876 (1989)
10. H. Li, H.R. Telle: IEEE J. QE-**25**, 257 (1989)
11. K.B. MacAdam, A. Steinbach, C.E. Wieman: Am. J. Phys. **60**, 1098 (1992)
12. G. Meisel, K.C. Harvey, A.L. Schawlow: Bull. Am. Phys. Soc. **19**, 580 (1974)
13. R. Grimm, J. Mlynek: Appl. Phys. B **49**, 179 (1989)

14. A.M. Akulshin, V.L. Velichansky, R.G. Gamidov, A.P. Kazantsev, V.A. Sautenkov, G.I. Surdotovich, V.P. Yakovlev: (FIAN, Moscow 1989) Preprint 122
15. A.M. Akulshin, A.A. Celikov, V.L. Velichansky: *Opt. Commun.* **84**, 139 (1991)
16. M. Ohtsu, K. Nakagawa, M. Kouroggi, W. Wang: *J. Appl. Phys.* **73**, R1 (1993)
17. J.E. Thomas, W.W. Quiver, Jr.: *Phys. Rev. A* **22**, 2115 (1980)
18. E. Arimondo, G. Orriols: *Il Nuovo Cimento* **17**, 333 (1976)
19. G. Alzetta, A. Gozzini, L. Moi, G. Orriols: *Il Nuovo Cimento* **36 B**, 5 (1976)
20. G. Alzetta, L. Moi, G. Orriols: *Il Nuovo Cimento* **52 B**, 209 (1979)
21. A. Aspect, E. Arimondo, R. Kaiser, N. Vansteenkiste, C. Cohen-Tannoudji: *Phys. Rev. Lett.* **61**, 826 (1988)